Rapid energy equilibration and emission of H and He in the reaction of 340-MeV ^{40}Ar with ^{197}Au

D. Logan
Department of Chemistry, Carnegie-Mellon University, Pittsburgh, Pennsylvania 15213

M. Rajagopalan
Department of Chemistry, State University of New York at Stony Brook, Stony Brook, New York 11794

M. S. Zisman
Lawrence Berkeley Laboratory, Berkeley, California 94720

John M. Alexander
Department of Chemistry, State University of New York at Stony Brook, Stony Brook, New York 11794

Morton Kaplan
Department of Chemistry, Carnegie-Mellon University, Pittsburgh, Pennsylvania 15213

Ludwik Kowalski
Montclair State College, Upper Montclair, New Jersey 07043

(Received 13 September 1979)

Energy and angular distributions have been measured for H and He both in singles and in coincidence with a heavy fragment. Large cross sections have been observed for both a low-temperature component at backward angles and a high-temperature component at forward angles. Both the preequilibrium and evaporationlike components are apparently emitted prior to scission, predominantly in coincidence with fragments of $Z > 27$. The angular anisotropy and out-of-plane correlation for ^{4}He are not consistent with emission from the composite systems of highest spin ($\approx 190\ \hbar$) but are consistent with emission from the ^{237}Bk composite with average spin $\approx 70\ \hbar$. Extensive energy sharing and H/He emission occur in many reactions so rapidly as to precede fission which is heavily favored by energetic and phase space considerations.

[NUCLEAR REACTIONS ^{197}Au(^{40}Ar, fission and H/He), $E = 340$ MeV, measured energy and angular distributions for ^{1,2,3}H and ^{4}He in singles mode and coincidences between H/He and one fission-like fragment.]

I. INTRODUCTION

Studies of light charged particle emission have provided many very interesting views of reactions between complex nuclei. In most cases, both an evaporative component and a direct component have been identified by their characteristic angular and energy distributions.[1-15] The energy distributions of the evaporative component give information on nuclear temperatures[1-15] and effective barriers to emission.[1,3,7-9,16-19] Their angular distributions give information on the angular momenta involved.[1,5,7-9,18,20-22]

The direct emission can involve a significant fraction of the reaction cross section. For light projectiles of Z up to 10 this contribution has been observed to increase rapidly with incident energy.[3,9,12-15] In reactions such as ^{16}O + ^{209}Bi, Britt and Quinton found direct ^{4}He emission to be favored near the grazing angle and with velocities close to that of the projectile.[3] On this basis they argued that projectile breakup may be responsible for such reactions. By contrast, for ^{159}Tb(^{14}N, αxn) reactions, Inamura *et al.*[10] observed similar forward-peaked ^{4}He angular distributions and cross sections but found that the resulting projectile residue fused with the target. Both studies, however, have indicated that such reactions are associated with the higher angular momenta. Recently, coincidence measurements have been made between γ rays and high-energy ^{4}He at forward angles.[11,13,14] These studies also confirmed that large cross sections for (HI, $\alpha xn\gamma$) reactions via direct mechanisms are associated with the larger partial waves in the entrance channel.

The high-energy H and ^{4}He emission at forward angles was found by Galin *et al.*[9] to be strong for ^{14}N + Rh but totally absent for ^{40}Ar + ^{77}Se. This result is suggestive of the idea that only the lighter projectiles give rise to the direct ejection of H and He. By contrast, however, recent coincidence studies have indicated such direct processes in high-energy quasielastic and deeply inelastic reactions (^{32}S + Au and ^{86}Kr + Au).[15,23] In both of

these reactions direct ^{4}He ejection was identified at forward angles possibly focused by the Coulomb fields of the separating fragments. In the ^{86}Kr induced reaction, prescission H and He emission were found, in addition, at backward angles and with rather low temperatures (≈3 MeV).[24]

Very interesting angular correlations both in and out of the reaction plane have also been reported for the reactions (^{16}O, ^{12}Cα) with Al, Ni, and Pb.[25-27] For both Al and Ni, direct ^{4}He emission is strongly favored in the reaction plane. Apparently the spin vector of the composite system is dictating this correlation even for the very rapidly ejected ^{4}He. An unexpected preference for out-of-plane emission has been observed for H in deeply inelastic reactions of ^{86}Kr with Au.[24]

These coincidence studies for deeply inelastic reactions are very interesting indeed. In order to understand them, however, we need to improve our background understanding for angular correlations in more simple reactions. At present, our knowledge is limited to anisotropies in compound nucleus reactions[1-9,21,22] and to the angular correlations of long-range particle emission in fission.[28,29] For the compound nucleus studies, clear separation of the roles of temperature and spin has rarely been achieved,[1-9,21] and for fission we only have data at excitations up to ≈40 MeV.[30]

We have chosen to study H and He emission in the reaction ^{40}Ar + ^{197}Au at 340 MeV; here sizable cross sections have been observed for fragments of $Z < 30$ (forward peaked) and also for heavier products that are emitted with $(1/\sin\theta)$ angular distributions.[31-34] The latter reactions seem to have all the characteristics of fission although the liquid-drop fission barrier is calculated to vanish even for rather low spins.[35] Some workers have chosen to identify the cross section for $30 \leq Z \leq 67$ with a "slow" fission process and to use this cross section to define a value of the critical l for fusion $[\sigma = \pi\lambda^2(l_{cr}+1)^2]$.[36] Others have argued that the distinction between fission and deeply inelastic reactions is not clear[31] and thus the meaning of such a value of l_{cr} is obscure. Recently a mechanism between fission and deeply inelastic reactions has been proposed[37] that can account for a relatively long lifetime for a composite system which is unstable to symmetric fission. It may be that the reaction system ^{40}Ar + ^{197}Au is therefore of special interest as an intermediate between those for very heavy reactants (e.g., ^{86}Kr + ^{209}Bi) where no complete fusion is clearly identifiable and those for lighter reactants (e.g., ^{12}C + ^{182}W) where the fusion cross section (and l_{cr}) is identified by fission plus evaporation-residue formation. Our hope is that the characteristics of emission of direct and/or evaporative H/He for the ^{40}Ar + ^{197}Au system will help to provide a link between the information from fission and evaporation studies at medium energies and the deeply inelastic reactions between heavier nuclei.

The specific questions we ask are as follows:

(1) What is the nature of the H/He emission and with what reaction products is it associated?

(2) Does emission of H/He precede or follow the scission of the composite nuclear system?

(3) To what extent has the translational energy of the entrance channel been damped in these processes?

(4) What information do the H/He energy spectra give regarding the energy sharing among particles in the composite system?

(5) What can be inferred about the angular momenta involved from the angular distributions of H/He?

(6) Can one account for the cross sections for fission and H/He emission (at back angles) by an equilibrium statistical model?

(7) What are the characteristics of H/He emission at forward angles and how do they compare with those in other reaction systems?

II. EXPERIMENTAL ARRANGEMENT

The 340-MeV ^{40}Ar beam from the Lawrence Berkeley Laboratory SuperHILAC was defined by two four-jaw collimators (2 mm×2 mm) and an antiscattering shield. Beam intensity was measured by a Faraday cup and two fixed monitor detectors after traversal of the Au target of thickness 1.25 mg/cm^2. Fission-like and projectile-like fragments were detected with a gas ionization telescope (GT) (Ref. 38) operated with methane gas at 15 torr and a polypropylene window of 35 μg/cm^2. The angle of this telescope with respect to the beam was denoted θ_G. The direction from target to GT and the beam line define the reaction plane for light particles detected in coincidence with heavy fragments. The 500 μm Si stopping detector in the GT was calibrated for energy and pulse-height defect with fission fragments from ^{252}Cf and the elastically scattered beam.[39] Atomic numbers (Z) for the fragments were determined relative to the elastically scattered ^{40}Ar by reference to the Northcliffe-Schilling tables.[40] For the main emphasis of this study we divide the fragments into two groups: (a) $Z \leq 27$ and (b) $Z > 27$. Earlier work has shown that the former group has a distinctly forward-peaked angular distribution, while for 248-MeV ^{40}Ar, the latter group seems to be symmetric about 90 deg c.m.[31-34]

The H and He particles were detected by two three-member solid state telescopes (SST) (45 μm, 500 μm, 5 mm Si detectors) mounted on an out-of-

plane arm. We describe the telescope positions by an angle in the reaction plane (θ_S) (0–360 deg) and an angle with respect to the reaction plane (φ). This out-of-plane angle should not be confused with the azimuthal angle in a spherical coordinate system. The telescopes were separated by $\Delta\varphi = 28$ deg and each had ≈10 msr solid angle acceptance. The c.m. angle with respect to the beam $\theta_{c.m.}$ and the c.m. energy ϵ are functions of both θ_S and φ as well as the measured lab-system energy. With the GT fixed at $\theta_G = 40°$ and 60° we swept the light particle telescopes from $100° < \theta_S < 339°$. We used a Ni foil (51 mg/cm^2) to stop the scattered beam for $\theta_S = 320°$ and 339°; for more backward angles only a thin cover foil was used (0.2 mg/cm^2 Au). Energy thresholds for detection and identification of H and He were 2 and 8 MeV for the thin cover foil and 5 and 20 MeV for the thick one. Events were recorded simultaneously from each telescope in the singles mode and in the coincidence mode between the GT and each SST. The coincidence measurements were made with time-to-amplitude converters (TAC's) and exhibited overall resolving times of ~30 nsec. The chance coincidence rates were easily distinguishable from true events in the TAC spectra and were negligible in comparison to the prompt peak. In the computation of absolute cross sections we assumed a charge state of +18 for the 340-MeV ^{40}Ar beam particles collected in the Faraday cup.

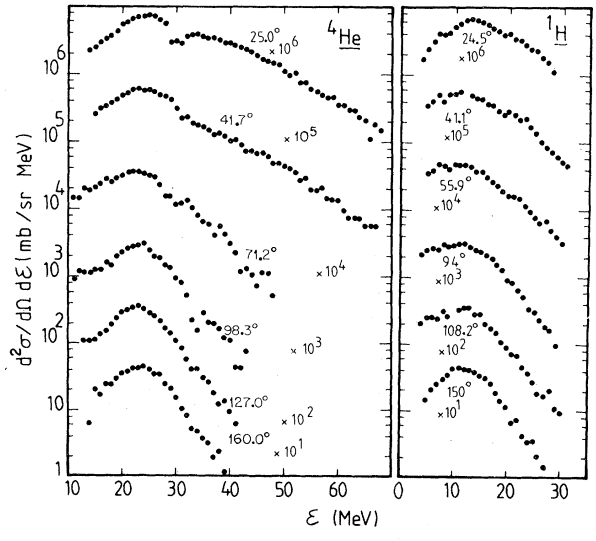

FIG. 1. Singles energy spectra in the c.m. for ^{4}He and ^{1}H at various angles. The average c.m. angle is indicated. Parameters describing the spectra are given in Table I.

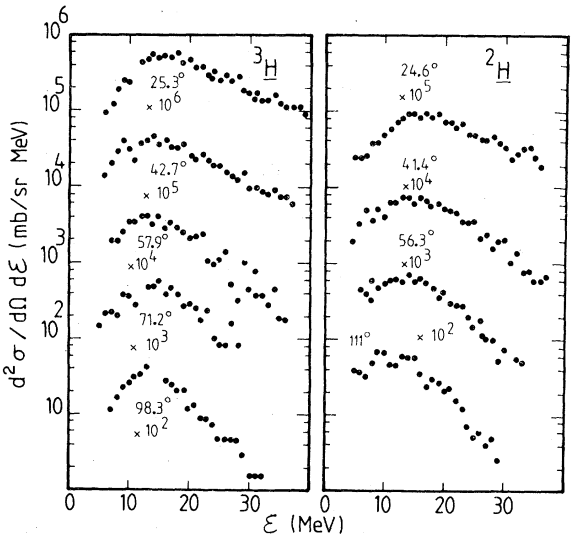

FIG. 2. Energy spectra for ^{2}H and ^{3}H as in Fig. 1.

III. RESULTS AND BRIEF DISCUSSION

The purpose of this section is to make a brief presentation of the body of experimental data that has been collected. In Sec. IV we will discuss the implications of the results in terms of the reaction mechanisms. Representative c.m. energy spectra for He and H in the singles mode are shown in Figs. 1 and 2 and parametrized for comparative purposes in Table I. Some technical problems could have flawed the energy measurements for particles that barely entered the third member of the solid state telescopes. Therefore we are doubtful of the reality of the minima shown in the spectra at forward angles. However, the more important features are unmarred: the evaporation-like spectra at back angles and the increasing quantity of high-energy H and He at forward angles. Angular distributions for He and H in the singles mode are shown in Figs. 3 and 4. Each particle distribution shows prominent forward peaking characteristic of direct mechanisms. For c.m. angles greater than 100 deg the production of ^{1}H becomes isotropic and that for ^{4}He shows a modest backward peaking, both of which could characterize statistical nuclear evaporation from an equilibrated system. For ^{2}H and ^{3}H the forward peak comprises a greater fraction of the total emission probability and direct mechanisms could contribute significantly even for $\theta_{c.m.} \sim 100$ deg. In Fig. 5 we compare typical back-angle spectra for ^{4}He and ^{1}H observed here with corresponding spectra from ^{194}Hg compound nuclei formed in several reactions.[12,19] The general shapes of the spectra are very similar and appear

TABLE I. Parameters that characterize the singles spectra.

^{4}He				^{1}H			
$\langle\theta_{c.m.}\rangle$ (deg)	ϵ_{mp} [a] (MeV)	FWHM [b] (MeV)	T [c] (MeV)	$\langle\theta_{c.m.}\rangle$ (deg)	ϵ_{mp} [a] (MeV)	FWHM [b] (MeV)	T [c] (MeV)
160	23.5	11	2.3 ± 0.2	150	12	12	2.5 ± 0.2
150	23	11	2.4 ± 0.2	127			2.6 ± 0.2
127	23	10	3.2 ± 0.2	109	12		2.6 ± 0.2
98	23.5	12	3.6 ± 0.5	95	12	14	3.0 ± 0.5
71	22	13	3.7 ± 0.5	73	12	16	3.3 ± 0.5
57	25		6.0 ± 0.5	56	11		4.1 ± 0.5
48	25	13	6.1 ± 0.5	41	12	16	3.9 ± 0.5
42	25	14	6.4 ± 0.5	25	13	14	4.4 ± 0.5
25	25	17	6.9 ± 0.5				
	^{2}H				^{3}H		
151			2.6 ± 0.3	98	14	13	3.6 ± 0.3
111	12	13	2.9 ± 0.3	49	15	13	4.9 ± 0.5
97	12	12	3.2 ± 0.3	43	14	17	6.9 ± 0.5
56	13	15	4.6 ± 0.5	25	15	17	7.1 ± 0.5
41	15	17	4.6 ± 0.5				
25	16	18	5.9 ± 0.5				

[a] The midpoint of the full width at half maximum; estimated uncertainty ~1 MeV.
[b] FWHM ≡ full width at half maximum; estimated uncertainty ~1 MeV.
[c] These values of T (temperature) are from fits of the spectra to the function $(\epsilon - B) \times \exp(-\epsilon/T)$ with $B = 23$, 12, and 11 MeV for ^{4}He, ^{1,2}H, and ^{3}H, respectively. (If B is reduced by 25%, then T for ^{4}He at 160 deg and for ^{1}H at 150 deg are both increased to 2.9 MeV).

to be typical evaporation spectra from systems of comparable temperature (high-energy slopes).

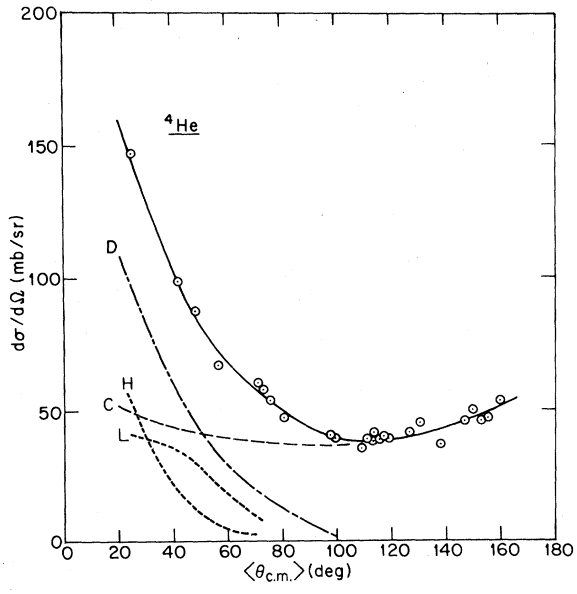

FIG. 3. Angular distribution for ^{4}He in the singles mode. Data are shown as points; the symmetric component is indicated C; the forward-peaked component by D. The forward-peaked component is broken into a high-temperature part H and a low-temperature part L.

For the ^{40}Ar + ^{197}Au reaction, both the ^{4}He and ^{1}H spectra in Fig. 5 are somewhat broader and shifted

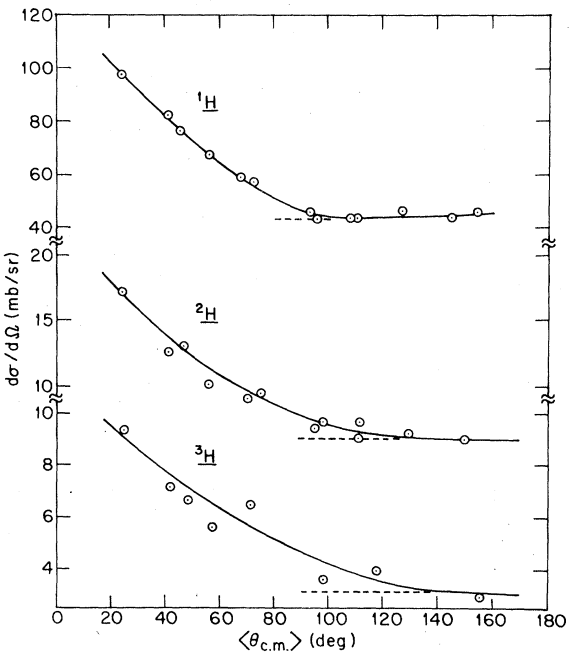

FIG. 4. Angular distributions for ^{1,2,3}H in the singles mode.

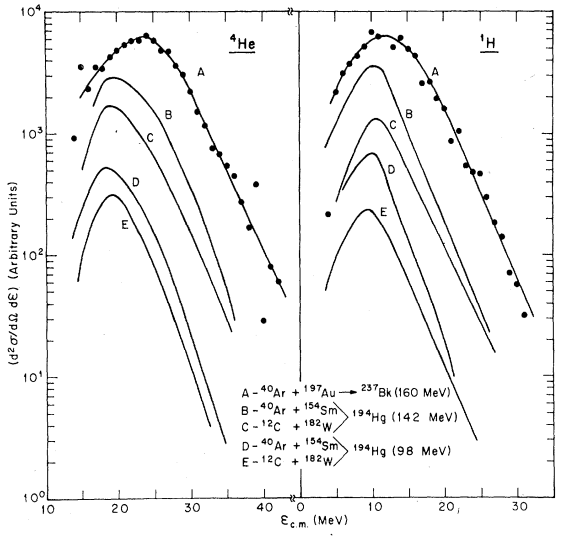

FIG. 5. Energy distributions for ^{4}He and ^{1}H at $\langle\theta_{c.m.}\rangle = 160°$ and 150°, respectively. These are compared to spectra from reactions leading to ^{194}Hg as shown ($\langle\theta_{c.m.}\rangle \sim 150$–$165°$). The ^{194}Hg data are from Ref. 12.

to higher energies, compared to the ^{194}Hg data. These significant differences will be discussed more fully in Sec. IV.

In Fig. 3 we have decomposed the angular distribution of ^{4}He particles into a "direct" component (labeled *D*) and an "evaporative" component (labeled *C*), making use of the theoretical requirement of symmetry about $\theta_{c.m.} = 90$ deg for emission from an equilibrated system. In the theory of nuclear evaporation,[18,20-22] the deviations from angular isotropy are related to angular momentum effects associated with the particle emission and depend on the spin of the emitter $(I_0 + \frac{1}{2})$, the orbital angular momentum of the emitted particle $(l + \frac{1}{2})$, and the spin-cutoff factor σ^2 in the nuclear level density. We have collected in Table II a set of relevant parameters calculated for ^{4}He evaporation from equilibrated ^{237}Bk systems of various assumed spins $(I_0 + \frac{1}{2})$. The details of the calculations and the inferences to be drawn from the results in Table II will be described in Sec. IV.

In this study we have made an initial survey of the correlations between H/He emission and one heavy fragment detected at 40° or 60° in the laboratory. As our objective was to get an overall view of the coincidence pattern, the angular coverage was rather extensive but the number of detected events was quite modest. A complete summary of the characteristics of the ^{1}H/^{4}He particles detected in the coincidence mode is given in Tables III–VI and Figs. 6 and 7. Table III presents the basic coincidence data for each angular configuration. For each measurement we have computed the average c.m. energies $\langle\epsilon_{c.m.}\rangle$ for ^{4}He and ^{1}H and the double differential cross sections $(d^2\sigma/d\Omega_S d\Omega_G)$, and these are listed in Table III. The coincidence angular distributions are displayed in Fig. 6 and the energy spectra,

TABLE II. Parameters related to the angular momenta for ^{4}He emission from an equilibrated ^{237}Bk composite system.

340-MeV ^{40}Ar + ^{197}Au → ^{237}Bk
$l_{max} = 190\ \hbar$; $E^* = 160$ MeV; $\hbar^2/2\mathcal{I} = 4.0$ keV

$(I_0+\frac{1}{2})$ ($\hbar$)	E_{rot} [a] (MeV)	U [b] (MeV)	T [c] (MeV)	$2\sigma^2$ [d]	$\langle(l+\frac{1}{2})^2\rangle^{1/2}$ [e] ($\hbar$)	β_1 [f]	β_2 [g]	$(\xi+2T)$ [h] (MeV)
0	0	144	2.5	605	7.4	0	0	5.0
50	10.0	134	2.4	584	8.1	0.70	0.38	6.0
70	19.6	125	2.3	563	8.9	1.11	0.78	7.0
90	32.4	112	2.2	533	9.9	1.67	1.36	8.3
100	40.0	104	2.1	515	10.5	2.03	1.74	9.0
115	52.9	92	2.0	482	11.4	2.73	2.47	10.3
190	144.3	0.1	0.1	15	17.0	222.	217.	17.3

[a] Computed from Eq. (17).
[b] Computed from Eq. (16).
[c] Computed from Eq. (15) with the level density parameter "a" = $(A/10)$ MeV^{-1}.
[d] As defined in Eq. (3).
[e] Obtained from Eq. (7).
[f] Obtained from Eq. (5′).
[g] Obtained from Eq. (13).
[h] The average total energy (above the barrier) due to thermal motions plus centrifugal spin-off as in Eq. (18).

TABLE III. Summary of coincidence results.

θ_S (deg)	φ (deg)	$\langle\theta_{c.m.}\rangle$ (deg)		$\langle\epsilon_{c.m.}\rangle$ (MeV)		Number of events [a]		$d^2\sigma/d\Omega_S d\Omega_G$ [b] (mb/sr^2)	
		^{4}He	^{1}H	^{4}He	^{1}H	^{4}He	^{1}H	^{4}He	^{1}H
				$\theta_G = 40$ deg					
100	0	112	109	21.4	11.1	12	7	8.4	4.7
	14	112	108	21.8	11.4	24	11	13.6	6.0
	28	111	108	21.6	11.7	21	20	11.1	10.3
	42	110	107	23.6	12.6	13	20	5.3	7.9
150	0	156	154	24.4	10.0	7	1	11.8	1.5
	14	153	152	23.8	10.3	4	3	6.0	4.0
	28	148	146	20.2	13.0	12	4	15.5	4.7
	42	139	138	22.5	11.4	5	6	4.8	5.3
255	0	116	112	26.7	13.8	18	8	12.5	5.3
	14	115	114	26.6	9.3	12	4	9.0	2.9
	28	114	111	27.5	13.8	15	19	7.7	9.4
	42	113	113	22.7	14.2	8	12	4.3	6.1
300	0	71	69	22.7	7.0	16	5	10.1	3.3
	14	72	69	22.7	11.4	28	9	11.1	3.8
	28	74	72	26.2	12.3	15	22	7.0	10.7
	42	80	78	23.2	11.7	23	13	6.8	4.0
320	0	46	46	28.1	9.9	27	9	16.6	5.7
	28	53	54	25.9	15.8	17	13	7.9	6.7
339	0	25	24	29.0	10.3	66	7	19.9	2.2
	28	40	40	24.3	13.3	33	33	7.5	8.3
				$\theta_G = 60$ deg					
120	0	131	127	23.2	12.1	19	16	4.2	3.0
	28	127	124	23.8	12.6	16	27	2.6	4.3
150	0	156	155	24.3	10.0	8	6	6.0	4.2
	28	147	144	24.3	14.7	11	9	5.8	4.3
205	0	160	158	23.1	15.3	11	6	6.9	3.2
	28	150	148	22.7	13.9	12	9	5.3	3.6
275	0	96	94	26.5	11.2	12	6	6.6	3.3
	28	98	95	23.7	12.1	10	10	4.1	4.1
300	0	71	68	22.8	10.0	11	5	5.8	2.8
	28	74	73	26.1	14.8	11	7	4.3	2.9
320	0	47	46	28.6	10.6	23	10	11.7	5.3
	28	54	54	25.3	16.2	14	18	5.5	7.6
339	0	25	24	25.1	11.3	31	8	13.6	3.8
	28	42	42	24.7	15.6	9	14	3.0	5.2

[a] Number of coincidence events recorded between light-particle telescopes (SST) at angle θ_S and heavy fragment telescope (GT) at angle θ_G. SST 1 subtended 9.1 msr and was used for the $\varphi = 0$ and $\varphi = 14$ deg measurements; SST 2 subtended 12.9 msr and was used at $\varphi = 28$ and $\varphi = 42$ deg.

[b] These cross sections have been transformed to the c.m. system only for the light particle (H/He); no transformation has been made for the heavy fragment.

grouped by angular region, are shown in Fig. 7. These figures together with the numbers of individual coincidence events in Table III give a feeling for the statistical uncertainties in the measurements. Yet within the limitations imposed by the statistics, it is apparent that the angular and energy distributions of the coincidence events are consistent with the measurements of ^{4}He/^{1}H in the singles mode (Figs. 1, 3, and 4). These observations suggest that the bulk of the light particles detected in the singles mode are also associated with the nuclear events detected in the coincidence

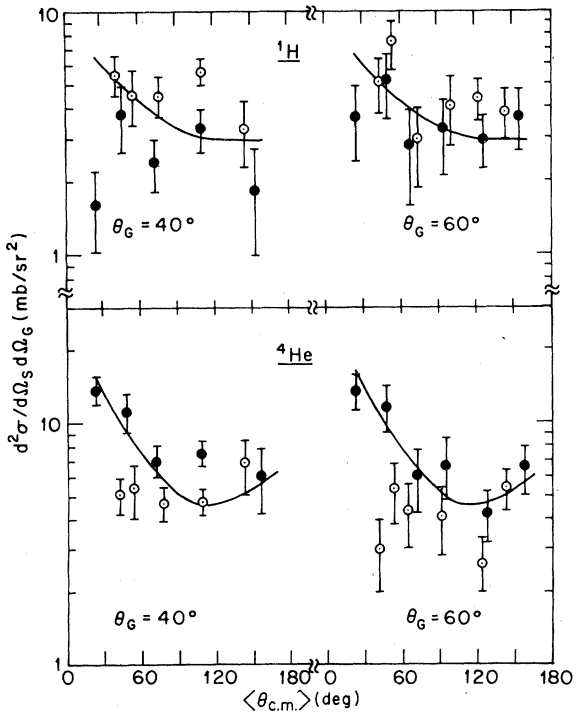

FIG. 6. Angular correlations for ^{4}He and ^{1}H with respect to heavy fragments detected in the gas telescope. The angle of the gas telescope is θ_G. The data for out-of-plane angles $\varphi = 28°$ and 42° have been averaged and are designated by open points (○). The data for $\varphi = 0°$ and 14° have likewise been averaged and are indicated by filled points (●). Data for $\theta_G = 40°$ have been normalized to that for $\theta_G = 60°$ by the relative fission cross sections (for comparative purposes). The smooth curves represent the shapes of the corresponding angular distributions in the *singles* mode. The data are from Table III with several points at similar c.m. angles combined.

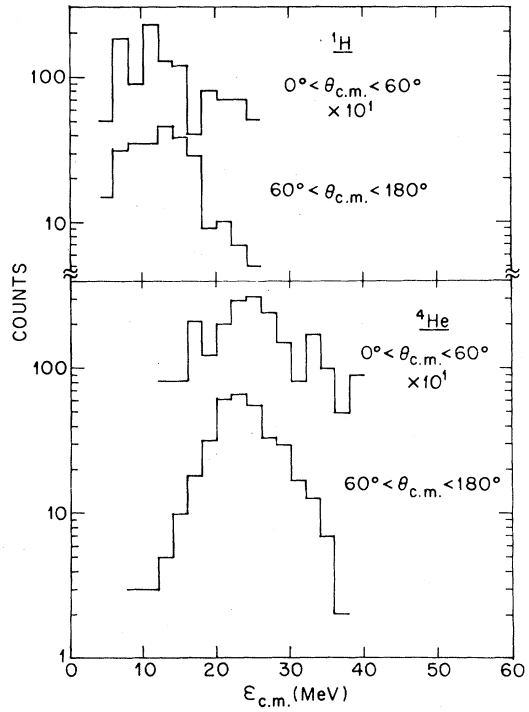

FIG. 7. Energy distributions (c.m.) for ^{1}H and ^{4}He observed in the coincidence mode with $\theta_G = 40°$ and 60°. All events observed are included and grouped according to the value of $\theta_{c.m.}$ for ^{1}H or ^{4}He.

mode.

For any coincidence study one must assess the kinds of reaction processes that are selected by the positions and thresholds of the detectors. For example, the study of Gamp *et al.* (373-MeV ^{32}S + Au) selected high-energy ^{4}He (>25 MeV) in coincidence with high-energy projectile-like fragments of $Z \leq 23$.[15] Their integrated coincidence cross sections constituted a small but very interesting fraction of the 800 mb of ^{4}He observed in singles. In this work we have used a gas telescope which could record fragments with $Z \geq 15$ and energies as low as ≈20 MeV. The trigger angle $\theta_G = 60°$ was well aft of the grazing angle and therefore it emphasized fission-like fragments of $27 < Z < 70$. For the smaller trigger angle $\theta_G = 40°$ a large number of projectile-like fragments was observed in singles from both quasielastic and very inelastic processes. Studies of elastic scattering give an estimate of ≈2.5 b for the reaction cross section,[3,41] and our results show that ≈1.4 b or ≈56% give fission-like fragments of $27 < Z < 70$. In Table IV we give the integrated cross sections for the forward and symmetric components of H/He detected in singles and the symmetric components detected in coincidence with a heavy fragment. As the angular distributions of the fission-like products have been found to follow $(\sin\theta_{c.m.})^{-1}$, we have integrated the coincidence cross sections with the aid of this symmetry condition (see Table IV footnote c and Ref. 22). Despite considerable uncertainties associated with the coincidence cross sections, it is clear that the symmetric components in singles and in coincidence are of comparable magnitudes. This result is strongly supportive of the suggestion that the coincidence experiments have been recording dominant processes for H/He production. Furthermore, the Z determinations from the gas telescope ($\theta_G = 40°$ and 60°) indicate that ≈90% of the fragments in coincidence with H/He have $27 < Z < 70$. Thus the major mechanisms for H/He emission involve fission-like reactions rather than quasielastic or deeply inelastic reactions that lead to projectile-like fragments.

Table V presents the coincidence data from

TABLE IV. Integrated light-particle cross sections (mb).

	Singles measurement		Coincidence measurement
	Symmetric component [a]	Forward component [b]	Symmetric component [c]
^{4}He	519	260	384
^{1}H	553	155	273
^{2}H	64	45	
^{3}H	(12.8) [d]	8.0	

[a] For ^{4}He the c.m. angular distribution was fitted to the function $W(\theta) = A\exp(-\gamma\theta) + B + C\cos^2\theta$, and the symmetric part ($B + C\cos^2\theta$) was integrated. For the H isotopes we assumed the symmetric component to be isotropic, and multiplied the back-angle cross sections (see Fig. 4) by 4π.

[b] These values were obtained by integration after subtraction of the symmetric component and linear extrapolation from $\theta_{c.m.} = 25$ to zero deg. (If we use an exponential extrapolation from 25 to zero deg, we get 290 mb for ^{4}He.)

[c] The cross sections ($d^2\sigma/d\Omega_S d\Omega_G$) from Table III at $\theta_G = 60$ deg and $\varphi = 0$ were averaged for all $\theta_{c.m.} > 60$ deg. Noting that $\theta_G = 60$ deg (lab) corresponds to $\theta_G = 90$ deg (c.m.), we transformed the averaged cross sections to the c.m. for the heavy fragment using an average factor 0.667 and then multiplied by π^2 to include all fission events. These values were then multiplied by 4π for ^{1}H and by 9.89 for ^{4}He to account for the apparent isotropy in ^{1}H emission and strong out-of-plane correlation in ^{4}He emission as described in Ref. 22.

[d] Poor statistics limited the determination of an effective temperature for ^{3}H at back angles. Therefore this cross section is more subject to the possible inclusion of contributions from high-temperature emissions.

Table III grouped to maximize the statistical significance and reveal differences between forward and backward emissions and between in-plane and out-of-plane coincidence events. Table VI gives the characteristics of the energy distributions for H/He, grouped by emission direction as Table V. From these tables, it appears that the cross sections and energies for ^{4}He and ^{1}H emitted out of the reaction plane ($\varphi = 28$ and 42 deg) are significantly different from the in-plane emissions ($\varphi = 0$ and 14 deg). We will discuss these correlations and the inferences to be drawn from them later in this paper. It can also be seen, particularly from Fig. 6 but also from Table V, that the major parts of the forward peaking in the H/He singles angular distributions are also reflected in the coincidence cross sections. Hence we conclude that the predominant fraction of the H/He recorded in the singles mode is emitted in coincidence with a heavy fragment and that ≈90% of these have $27 < Z < 70$. Only ≈10% of the coincidence events were found to be associated with a projectile-like fragment of $Z \leq 27$. Little if any cross section remains for H/He emission from residual nuclei that survive fission-like breakups.

The large probability for coincidence between H/He and fission-like products does not distinguish between H/He emitted from the ^{237}Bk composite system or from the separating products. To attempt such a distinction, we refer to the velocity vector diagram in Fig. 8 which represents ^{4}He evaporation from either of two fission fragments, as detected in coincidence with one of them. For the configuration shown (GT at 60° lab), the fission fragments are emitted at 90° in the c.m., and the ^{4}He particles were recorded by SST's at the angles indicated. (For measurements with GT at 40° lab, the diagram is more complicated but similar.) The solid circle represents the laboratory energy threshold (8 MeV) of the SST's, and the dashed circles are the mean ^{4}He emission velocities in the moving frames of the respective fission fragments. Examination of Fig. 8 indicates two important points. First, the observed mean ^{4}He energies detected in coincidence with a fission

TABLE V. Ratios of total coincidence events and relative cross sections for $\varphi = 28$ and 42 deg to those for $\varphi = 0$ and 14 deg.

Span of c.m. angles (deg) [a]	$(N_{28+42})/(N_{0+14})$ [b]		$(\sigma_{28+42})/(\sigma_{0+14})$ [c]	
	^{4}He	^{1}H	^{4}He	^{1}H
60–180	172/182	178/87	0.72±0.10	1.52±0.18
0– 60	73/147	78/34	0.38±0.06	1.82±0.35

[a] Range of angles covered by the SST's.

[b] Ratios of numbers of coincidence events for θ_G of 40 and 60 deg combined.

[c] Ratios of summed numbers of events (corrected for dead-time effects) divided by the respective solid angles. These ratios are equivalent to average cross section ratios from Table III, with the averaging being weighted by the number of observed events at each angular configuration.

TABLE VI. First and second moments of the energy distributions for ^{1}H and ^{4}He detected in coincidence with heavy fragments.

$\langle\theta_{c.m.}\rangle$ (deg)	φ (deg)	^{1}H N^a	^{1}H $\langle\epsilon\rangle^b$ (MeV)	^{1}H $\sigma_\epsilon{}^b$ (MeV)	^{4}He N^a	^{4}He $\langle\epsilon\rangle^b$ (MeV)	^{4}He $\sigma_\epsilon{}^b$ (MeV)
			$\theta_G = 40$ deg				
<60	0–14	16	9.2	2.8	93	28.3	8.0
<60	28–42	46	13.7	5.5	50	24.0	7.6
>60	0–14	48	10.8	3.8	121	24.3	7.1
>60	28–42	116	12.7	5.2	112	23.2	6.1
			$\theta_G = 60$ deg				
<60	0	18	10.6	3.7	54	26.0	7.6
<60	28	32	15.1	6.7	23	23.7	4.7
>60	0	39	11.9	3.6	61	23.7	4.7
>60	28	62	13.1	4.7	60	23.6	4.3

[a] Number of events observed.

[b] $\langle\epsilon\rangle$ and σ_ϵ are, respectively, the first and second moments of the observed energy distributions (c.m.). Note that the standard deviation of the mean $\langle\epsilon\rangle$ is $\approx \sigma_\epsilon/\sqrt{N}$.

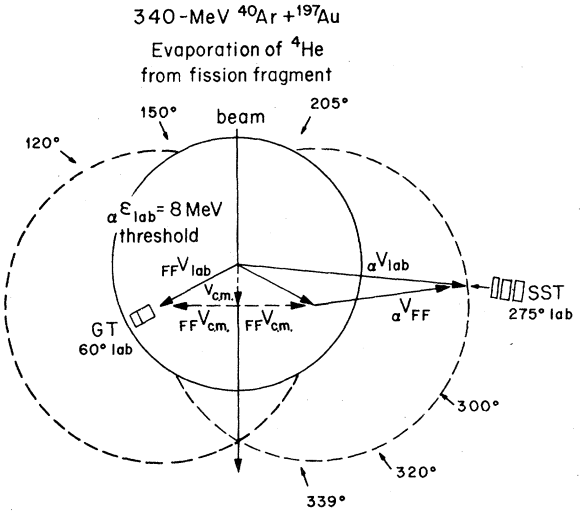

FIG. 8. Velocity vector diagram representing ^{4}He evaporation from either of two fission fragments, as detected in coincidence with one of them. The symbols are as follows: $_{FF}V$ and $_{\alpha}V$ are the mean velocities of a typical fission fragment or ^{4}He particle, respectively, with subscripts for laboratory or c.m. frames. $V_{c.m.}$ is the velocity *of* the center-of-mass, and $_{\alpha}V_{FF}$ is the ^{4}He mean velocity in the frame of the emitting fragment. The solid circle represents the laboratory energy threshold (8 MeV) of the light-particle detector (SST), and the dashed circles are the mean ^{4}He emission velocities in the respective fission fragment frames. For the configuration shown (GT at 60° lab), the fission fragments are emitted at 90° in the c.m., and ^{4}He particles were recorded in the SST at the angles indicated. The diagram indicates that the mean ^{4}He energies observed in coincidence should vary strongly with angle if emission occurs primarily from fully accelerated fission fragments. It is also apparent that the laboratory threshold (solid circle) would eliminate most ^{4}He particles evaporated from a fission fragment moving away from the SST direction.

fragment should vary strongly with angle if emission occurs primarily from the fully accelerated fragments. Second, the SST threshold of 8 MeV will effectively exclude (see solid circle) most ^{4}He particles evaporated from a fragment moving away from the SST direction. In the next section, we make quantitative comparisons between calculated and observed mean energies (as well as cross sections). It shall suffice here to say that the experimental data do not follow the trends with angle predicted for evaporation from moving fission fragments. In the case of ^{1}H emission, the corresponding velocity vectors are such that mean energies alone do not distinguish adequately between emission sources.

In addition, the shapes of the singles (noncoincidence) energy spectra of ^{1}H and ^{4}He can provide a means for distinguishing emission sources. In Fig. 9 we show results of a Monte Carlo simulation[42] of H/He emission from fully accelerated fission fragments. In the calculation we have assumed a Gaussian mass distribution of standard deviation 30 mass units centered about $A = 237/2$. Evaporation of H/He was assumed to be equally probable from each fragment. The calculated curves for ^{4}He in Fig. 9 are much wider than the measured spectra at corresponding angles in Fig. 1; thus this mechanism is clearly not dominant. For ^{1}H the calculated curves are steeper at high energies than the experimental ones and their angular dependence (Fig. 9) is also not reflected in the observed data. Therefore we are led to the interesting conclusion that most ^{4}He emission, and probably ^{1}H emission also, precedes full fragment acceleration. A more detailed discussion of this matter is given in the next section.

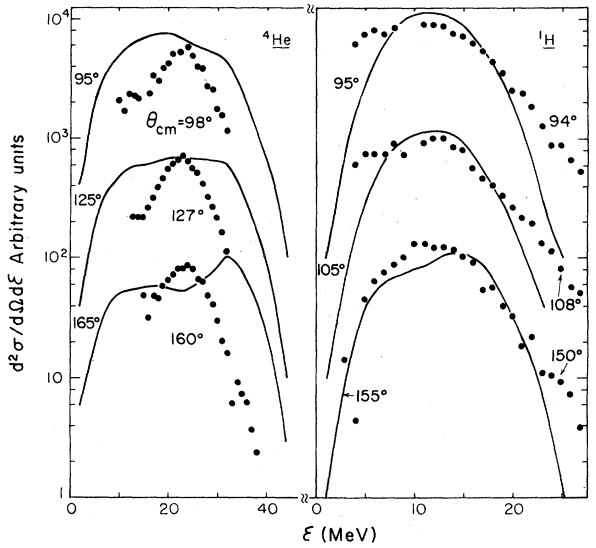

FIG. 9. Energy spectra for ^{1}H and ^{4}He calculated by a Monte Carlo simulation of evaporation from fission fragments (smooth curves). Gaussian distributions were assumed for the mass and total energy distributions in fission with standard deviations of 30 mass units and 15 MeV, respectively. Angular distributions (c.m.) for each fission product were taken to be $1/\sin\theta$ and isotropic for H/He. The evaporation spectra were taken from Eq. (1) with barrier parameters B from Ref. 19 and T from Eqs. (15) and (16). Experimental spectra are shown as points.

IV. MECHANISTIC IMPLICATIONS OF THE RESULTS

In the preceding section we considered the general features of the H/He emission and the nature of the reaction products with which it is associated. We showed that ≈90% of the coincident H/He emission is correlated with fission-like products of $27 < Z < 70$. In addition, the mean Z values for fragments detected in singles and in coincidence differ by less than three charge units. In the present work, we will focus on these prominent fission-like processes. The earlier work of Ref. 15 (373-MeV ^{32}S + Au) dealt with the small fraction of high energy ^{4}He in coincidence with projectile-like fragments ($Z \leq 23$).

We would now like to discuss in more detail the question of whether the H/He emission precedes or follows scission and full acceleration of the fragments. We have already described, using the vector diagram in Fig. 8, the significant kinematic shifts expected for ^{4}He emission from moving fragments. In Table VII we compare quantitatively the mean energies and also the cross sections from our coincidence measurements with the results obtained from Monte Carlo kinematic simulations. The calculations were carried out using the experimental laboratory detection thresholds, and assumed mass and the total energy distributions in fission to be Gaussian with standard deviations of 30 mass units and 15

TABLE VII. Charged particle emission in the reaction 340-MeV ^{40}Ar + ^{197}Au; comparison of mean energies and cross sections from coincidence measurements with results obtained from Monte Carlo kinematic simulations for evaporation from fully accelerated fission fragments.

	^{4}He				^{1}H			
θ_S	$\langle\epsilon_{lab}\rangle$ (MeV)		Lab cross section[a]		$\langle\epsilon_{lab}\rangle$ (MeV)		Lab cross section[a]	
(deg)	Calc.	Obs.[b]	Calc.	Obs.[b]	Calc.	Obs.[b]	Calc.	Obs.[b]
				θ_G = 40 deg				
100	22.8	19.5	5.6	10.1	12.8	10.6	1.9	4.9
150	13.8	16.6	2.3	6.6	8.8	7.5	1.5	2.7
255	25.9	23.3	10.2	8.6	12.6	11.6	3.5	3.6
300	29.3	26.5	14.2	14.2	14.5	11.8	4.6	4.6
320	27.1	36.0	10.5	20.8	13.8	12.1	4.7	6.9
339	26.5	39.4	9.9	27.4	14.5	13.4	4.1	2.9
				θ_G = 60 deg				
120	23.5	18.0	2.4	3.5	12.6	10.0	1.2	2.9
150	17.2	16.6	0.9	4.0	9.8	7.5	0.9	3.0
205	17.3	15.3	1.0	4.1	9.8	11.8	1.9	2.3
275	34.6	26.5	6.5	6.2	15.8	11.3	3.0	3.1
300	37.8	28.3	7.2	7.2	16.5	11.0	3.3	3.3
320	38.5	36.5	5.6	15.2	16.0	13.1	3.3	6.6
339	30.2	34.6	2.0	18.6	14.3	14.2	2.8	4.8

[a] $(d^2\sigma/d\Omega_S d\Omega_G)$ in units (mb/sr^2); the calculated cross sections have been normalized to the experimental results at θ_S = 300 deg for each case.

[b] Data for φ = 14 deg has been combined with that for φ = 0 deg where measured (see Table III).

MeV, respectively. The angular distributions were taken to be $(\sin\theta_{c.m.})^{-1}$ for the fission fragments and isotropic in the moving frame for H/He. Even though the statistics of the experimental coincidence measurements are relatively poor, the mean energies observed for each angle are determined to ±1–2 MeV, which is adequate precision to allow meaningful comparisons to be made in some, if not all, cases represented in Table VII.

Consider the ^{4}He data in Table VII. For both $\theta_G = 40°$ and $\theta_G = 60°$ there are clear differences between the calculated and observed average energies. The experimental data show a generally smooth decrease in average ^{4}He energy from forward angles to backward angles, whereas the calculations predict energy maxima in the directions associated with a moving fission fragment. Furthermore, the calculated cross sections are largest in the fragment directions and fall to much smaller values in unfavorable directions such as 150°, while in contrast, the observed coincidence cross sections increase continuously toward forward angles and do not exhibit the pronounced "deep hole" in the vicinity of 150°. For the ^{1}H data, the comparison of observed with calculated average energies is not so distinctive (the expected kinematic shifts are smaller), and one cannot readily discern systematic deviations clearly outside of experimental uncertainties. However, the ^{1}H cross section data do seem to show systematic differences in the magnitudes of the hills and valleys which, though less pronounced than for ^{4}He, are probably significant.

From the comparisons in Table VII and the arguments based on Figs. 8 and 9, we find there are four clear experimental observations that indicate the predominance of ^{4}He emission prior to significant fragment acceleration: (1) The average energies of ^{4}He in coincidence are not enhanced in the direction of either fragment. (2) The coincidence cross sections show no enhancement in the direction of either fragment, nor do they decrease for other directions (Table VII and Fig. 6). (3) The shapes of the singles energy spectra for $\theta_{c.m.} > 100°$ (Figs. 1 and 5) are quite different from those expected for isotropic emission from fully accelerated fragments (Fig. 9). (4) The shapes of the ^{4}He energy spectra observed in the coincidence mode are similar to those observed in the singles mode (Figs. 1 and 7). These four points apply also for ^{1}H emission but with much less force due to the expectation of smaller kinematic shifts.

Two more observations suggest that H/He emission occurs even before the act of scission: (5) The average energies are consistent with evaporation from a composite of total $Z \approx 97$ (Tables I, III, and VI and Figs. 5, 7).[19] In Fig. 5 the back-angle energy spectra are compared to those observed for the reactions $^{12}C + {}^{182}W$ and $^{40}Ar + {}^{154}Sm$ leading to ^{194}Hg excited to 98 and 142 MeV. The peak energies can be seen to be consistent with the Z ratio of 97/80. (For the ^{194}Hg system at 98 MeV less than 10% of H/He emission was found to be in coincidence with fission.[12]) (6) The ratio of He to H cross sections is ≈0.9 (for $\theta_{c.m.} > 100°$). This ratio would be expected to be ≈0.2 for a fragment of mass 78–117 with spin ≈20.[8,9,21,22] For such a fragment a spin of ≈60 would be implied by this He/H ratio of 0.9. Such large spins are well above estimates from the "sticking model." By contrast, this ratio is consistent with that of a compound nucleus ^{194}Hg (and by implication ^{237}Bk) of mean spin ≈60.[12,21] We conclude that the predominant fraction of ^{4}He emission (and probably ^{1}H also) precedes scission of ^{237}Bk even for this highly excited composite system which must have a very short lifetime.[43] (The abundance of H/He with energies below their most probable value may signify emission from a very deformed composite system,[37] but detailed calculation of the spectral shapes must be made to explore this point.[19])

To what extent has energy damping or relaxation occurred in the exit channels associated with H/He emission? In Ref. 15 (373-MeV $^{32}S + Au$) it was shown that forward-peaked high-energy ^{4}He emission occurs in coincidence with quasielastic reactions giving projectile-like residues. In the present work we have shown that ≈90% of the coincident H/He emission is with fission-like products ($27 < Z < 70$). The energies of these fission-like fragments are typical of the gross fission product distribution with average c.m. energies ≈90 MeV. In short, the exit channel heavy fragment energies are for the most part, completely damped. Hence we can infer that for these fragments the memory of the entrance channel was largely erased by complex processes of energy, charge, and mass exchange.

What information do the H/He energy spectra give regarding the energy sharing among particles in the composite system? We have seen that the H/He emission precedes a fission-like breakup with complete energy damping in a composite system which must not live longer than several nano-picoseconds.[43] The energy spectra of H/He at forward angles have many high-energy particles with velocities near those of the projectile (Figs. 1, 2, and 7). Presumably these emissions reflect a memory of the projectile's speed and relatively little energy mixing with other constituents of the intermediate complex. It is convenient

to discuss the energy mixing more generally in terms of effective temperatures as a function of angle.[11] We have made fits of the spectra in Figs. 1 and 2 to the functional form:

$$P(\epsilon) = (\epsilon - B)\exp(-\epsilon/T), \quad (1)$$

where B and T are the effective barrier and temperature, respectively. These fits are not useful for the lower energies but can provide a parameter T to characterize the high-energy tail of each spectrum. The values of T are given in Table I along with "peak" energy and width parameters to characterize the spectrum at each angle. We see that these spectral parameters become independent of angle for $\theta_{c.m.} > \sim 100°$ for ^{1}H and $\sim 127°$ for ^{4}He. The T values for ^{1}H and ^{4}He are both ≈ 2.5 MeV, a value very close to that observed for ^{194}Hg compound nuclei excited to 100–140 MeV.[12,19] (See Fig. 5.) Such low temperatures imply essentially complete energy mixing among the H and He particles in the intermediate complex. Similarly the "peak" energy is $\approx 15\%$ greater than that observed for the system ^{194}Hg. This is as expected from the relevant Coulomb barrier ratio for the two systems. In short, these H/He emissions at back angles have energy and angular distributions that are consistent with an equilibrated compound nucleus, a remarkable result for a system of such high charge, energy, and spin (Figs. 3–8).

McMahan and Alexander have shown that for the ^{194}Hg system ($E^* = 98$ MeV) the barrier to evaporation is $\approx 10\%$ lower than the barrier to fusion.[19] The widths [full width at half maximum (FWHM)] of the particle energy spectra from the ^{237}Bk composite are ≈ 12 MeV compared to about 8 MeV for ^{194}Hg (see Fig. 5). This additional width for ^{4}He and the low-energy shelf for ^{1}H (Fig. 1) could imply significant emission from a very deformed complex or from a neck between fragments. This could then offer a very interesting possibility for studying the composite system at an early stage in its evolution toward scission.

The spectra at forward angles are characterized by a high-temperature component that seems to reflect a memory of the projectile's speed. In addition, however, there are many H/He particles with near-barrier energies at the forward angles. Their abundance is significantly larger than that obtained by reflection symmetry of the back-angle spectra about $\theta_{c.m.} = 90°$. This may be illustrated in the case of ^{4}He. If one imagines that these forward-peaked particles can be decomposed into low (L) and high (H) temperature components, then the curves in Fig. 3 labeled L and H give a feeling for their relative magnitudes. Alternatively, of course, the processes of H/He emission may result from a continuum of effective temperatures and lifetimes of the composite system that are almost completely thermalized for $\theta_{c.m.} > \sim 100°$, but only partially thermalized for $\theta_{c.m.} < \sim 100°$.[44]

As a large fraction of the H/He emission appears to be characteristic of evaporation from an essentially equilibrated system, it is of interest to consider the observed angular distributions and correlations as probes of the angular momenta. To do this we shall first make some estimates of the theoretical angular and energy correlations, using the relationships derived from the statistical model for nuclear evaporation.[18,20-22] Following the treatment given by Ericson and Strutinski[20] (but using semiclassical approximations for the magnitudes of the various angular momenta[21,22]), there is a correlation of emission probability $W(\varphi^*)$ with the angle φ^* between the emitted particle of energy ϵ and orbital angular momentum $(l+\frac{1}{2})\hbar$ and the angular momentum of the emitter $(I_0+\frac{1}{2})\hbar$:

$$W_{I_0,l,\mathcal{J}T}(\varphi^*) \propto J_0\left(\frac{i(I_0+\frac{1}{2})(l+\frac{1}{2})}{\sigma^2}\sin\varphi^*\right). \quad (2)$$

In this equation $J_0\{x\}$ is the zero-order Bessel function of argument x and σ^2 is the spin-cutoff factor in the nuclear level density given by

$$\sigma^2 = \mathcal{J}T/\hbar^2, \quad (3)$$

where $\mathcal{J}$ and T are the moment of inertia and the temperature of the residual nucleus. One must recognize that Eq. (2) applies when the angular momentum of the emitter has a unique orientation in space, as might be selected by the requirements of a coincidence experiment. Our experimental out-of-plane angle φ can be related to φ^* in Eq. (2) if we identify the spin of the emitter with the normal to the reaction plane. In this case, $(\pi/2 - \varphi)$ transformed to the c.m. system is φ^*. The specification of $\mathcal{J}T$ or σ^2 in Eq. (2) requires selection of particular emissions (e.g., E^*, ϵ, etc.) and a knowledge of the level density. For an ensemble of nuclei with angular momenta uniformly distributed perpendicular to the beam axis (as might be expected in observations with a single detector in a compound nucleus reaction), particles will be emitted at angles θ with respect to the beam:

$$W_{I_0,l,\mathcal{J}T}(\theta) \propto \sum_{k=0}^{\infty}(-)^k(4k+1)j_{2k}\left(\frac{i(I_0+\frac{1}{2})(l+\frac{1}{2})}{\sigma^2}\right) \times [P_{2k}(0)]^2 P_{2k}(\cos\theta), \quad (4)$$

where j_{2k} and P_{2k} are, respectively, a spherical Bessel function and Legendre polynomial of order $2k$. Equations (2) and (4) depend only on the parameter $\beta_1 = (I_0+\frac{1}{2})(l+\frac{1}{2})/2\sigma^2$. On expansion of Eqs. (2) and (4) the first term is of order β_1^2:

$$\beta_1^2 = \frac{(I_0+\frac{1}{2})^2(l+\frac{1}{2})^2}{(2\sigma^2)^2}, \quad (5)$$

and therefore the root-mean-square values of $(I_0+\frac{1}{2})$ and $(l+\frac{1}{2})$ are of primary importance. For I_0 values of any practical interest, one must consider the distribution of l values and we may use the relation given by Døssing[21]:

$$P_{I_0,\mathcal{I}T}(l)\propto\left\{\exp\left[\frac{(I_0+\frac{1}{2})(l+\frac{1}{2})}{\sigma^2}-\frac{\hbar^2(l+\frac{1}{2})^2}{2T\mu R^2}\left(\frac{\mathcal{I}_\perp}{\mathcal{I}}\right)\right]\right\}\times\left\{1-\exp\left[-\frac{2(I_0+\frac{1}{2})(l+\frac{1}{2})}{\sigma^2}\right]\right\},\tag{6}$$

where μ is the reduced mass of the emitted particle, and R and T are the radius and temperature of the residual nucleus. Also, $\mathcal{I}_\perp=\mathcal{I}+\mu R^2$, and one should note that μR^2 refers to the centrifugal barrier for evaporation. Because of Eq. (5), the most important average related to $P_{I_0,\mathcal{I}T}(l)$ in Eq. (6) is the quantity $\langle(l+\frac{1}{2})^2\rangle$. Catchen *et al.*[22] have derived an exact expression for this average:

$$\langle(l+\tfrac{1}{2})^2\rangle=\frac{[1+(\gamma^2/2)]\,\mathrm{erf}(\gamma/2)+(\gamma/\sqrt{\pi})\exp(-\gamma^2/4)}{2b\,\mathrm{erf}(\gamma/2)},\tag{7}$$

where

$$\gamma=(I_0+\tfrac{1}{2})/b^{1/2}\sigma^2=\eta(I_0+\tfrac{1}{2}),\tag{8}$$

$$b=\hbar^2\mathcal{I}_\perp/2\mu R^2\mathcal{I}T,\tag{9}$$

and

$$\eta=(2\mu R^2\hbar^2/\mathcal{I}\mathcal{I}_\perp T)^{1/2}.\tag{10}$$

From these equations, one can see that the quantity $\langle(l+\frac{1}{2})^2\rangle b$ is a function only of I_0 for a given value of η.

Equations (2) and (4) are strictly applicable for one value of $\beta_1=\hbar^2(I_0+\frac{1}{2})(l+\frac{1}{2})/2\mathcal{I}T$ and therefore for distributions of I_0, l, and/or $\mathcal{I}T$ one should take the most appropriate average or specifically perform the summations of interest. Our approach here is to estimate

$$\beta_1{}^2=\frac{\langle(I_0+\frac{1}{2})^2\rangle\langle(l+\frac{1}{2})^2\rangle}{(2\sigma^2)^2}\tag{5′}$$

and use it in Eqs. (2) and (4). A second approach is to weight Eqs. (2) and (4) appropriately and sum over the spectrum of l and ϵ for the evaporated particles. Using standard approximations Døssing has carried out such integrations.[21] Analogous to Eq. (2) he obtains

$$W_{I_0,\mathcal{I}T}(\varphi^*)\propto\exp(\beta_2\sin^2\varphi^*),\tag{11}$$

and analogous to Eq. (4) he finds

$$W_{I_0,\mathcal{I}T}(\theta)\propto[\exp(-\beta_2\sin^2\theta/2)]J_0(i\beta_2\sin^2\theta/2),\tag{12}$$

where

$$\beta_2=\frac{(I_0+\frac{1}{2})^2}{2\sigma^2}\left(\frac{\mu R^2}{\mathcal{I}_\perp}\right).\tag{13}$$

Either Eq. (2) or Eq. (11) can be used to interpret angular correlations of emitted particles with respect to a unique spin vector. Correspondingly, Eqs. (4) or (12) should apply to angular distributions measured with respect to the beam in compound-nucleus experiments, since here no unique reaction plane is defined and the spin vectors of the emitting nuclei are uniformly distributed in (or close to) a plane perpendicular to the beam direction. In either case, attention must be given to the appropriate choice of the parameters β_1 and β_2. These parameters may be computed theoretically as functions of $(I_0+\frac{1}{2})$ using the equations given above. Implicit in such a calculation is the assumption that the particle emission occurs at the first step of the evaporation chain. We also require absolute estimates of $\mathcal{I}$, T, and μR^2 which we have made in the following manner. For μR^2 we use $\mu(1.42A^{1/3}\,\mathrm{fm}+R_p$ or $R_\alpha)^2$ as discussed in Ref. 19. The moment of inertia $\mathcal{I}$ we take as

$$\mathcal{I}=\tfrac{2}{5}Mr^2,\tag{14}$$

with M the mass of the nucleus and $r=1.2A^{1/3}$ fm (for the matter radius). The temperature is related to the average energy available for thermal excitation:

$$U=aT^2,\tag{15}$$

with "a" $=(A/10)$ MeV^{-1} and

$$U=E^*-\langle\epsilon\rangle-S-E_{\mathrm{rot}}.\tag{16}$$

The separation energy of the emitted particle is S and its average kinetic energy $\langle\epsilon\rangle$ is taken to be $(B+2T)$, where B is the exit channel barrier.[19] The rotational energy E_{rot} and moment of inertia $\mathcal{I}$ refer to the emitting nucleus and are related by

$$E_{\mathrm{rot}}=\hbar^2(I_0+\tfrac{1}{2})^2/2\mathcal{I}.\tag{17}$$

We present in Table II a calculated set of the relevant parameters for ^{4}He evaporation from the system of interest here, 340-MeV ^{40}Ar + ^{197}Au $\rightarrow{}^{237}$Bk. For selected values of the emitter spin $(I_0+\frac{1}{2})$ listed in the first column, we give values of the quantities E_{rot}, U, T, $2\sigma^2$, $\langle(l+\frac{1}{2})^2\rangle^{1/2}$, β_1 and β_2 in columns 2–8, respectively. The last column in Table II represents the average total kinetic energy (above the barrier) of an evaporated particle, consisting of the average thermal energy $2T$ and a centrifugal part ξ from the rotating emitter

$$\xi=4E_{\mathrm{rot}}\mu R^2/3\mathcal{I}.\tag{18}$$

Several points should be noted from the results in Table II. For spins nearing the maximum en-

trance channel spin ($l_{max} = 190\ \hbar$), the rotational energy of a spherical nucleus would be very large and its temperature would be very small. An evaporated ^{4}He particle would have energy and angular correlations dominated by centrifugal spinoff. For spins $(I_0 + \frac{1}{2}) \lesssim 100\ \hbar$ the rotational energies are more modest and the values of T, $2\sigma^2$, and $\langle (l+\frac{1}{2})^2 \rangle^{1/2}$ are rather stable for various values of $(I_0 + \frac{1}{2})$. In this region of spins the variation in the angular correlation parameters β_1 and β_2 is dominated by the spin of the emitter and hence may be used as its signature. Both $\langle (l+\frac{1}{2})^2 \rangle^{1/2}$ and σ^2 are dependent on the size and shape of the residual nucleus, which are unknown. We make estimates with spherical shapes, but a generalization of Eqs. (14)–(17) to other shapes may lead to partially compensating changes in the ratio $\langle (l+\frac{1}{2})^2 \rangle / \sigma^4$. The average energy $(\xi + 2T)$ (over the barrier) in Table II is only slowly increasing with spin $(I_0 + \frac{1}{2})$ and provides no strong signature unless E_{rot} approaches E^*. Perhaps the higher-energy ^{4}He particles observed at $\theta_{c.m.} < 60$ deg could reflect such large spins.

Let us now consider the measured angular distributions. For the H isotopes the angular distributions in singles (at back angles) are essentially isotropic and no definitive information can be extracted (only a rather uninteresting upper limit). For the ^{4}He emission, however, we may use the experimental data to obtain estimates of β_1 and β_2. First we have fitted Eqs. (4) and (12) to the angular distribution in singles (Fig. 3, $\theta_{c.m.} > 100$ deg). This yields the values $\beta_1 = 1.0$ and $\beta_2 = 0.73$. Comparison with the theoretical estimates as given in Table II results in the spins $\langle (I+\frac{1}{2})^2 \rangle^{1/2} = 65\ \hbar$ from β_1 and $\langle (I+\frac{1}{2})^2 \rangle^{1/2} = 68\ \hbar$ from β_2. Each of these has a probable uncertainty of ~10% arising from the experimental fits alone. Quite independently, we could obtain additional estimates by fitting Eqs. (2) and (11) to the out-of-plane coincidence correlation data from Table V. Unfortunately, the quality of these data is relatively poor, and even though we have grouped the data in Table V to maximize the statistical significance, the uncertainty in derived parameters will be large. Using Eq. (11) we estimate $\beta_2 \approx 1.1 \pm 0.4$, which translates into spins $\langle (I+\frac{1}{2})^2 \rangle^{1/2} \approx 82 \pm 15\ \hbar$. This result, while imprecise, is not inconsistent with the analysis of the singles data. Thus we can conclude that a typical initial spin associated with equilibrium ^{4}He evaporation is $\langle (I+\frac{1}{2})^2 \rangle^{1/2} \approx 70\ \hbar$. It is rather clear that ^{4}He evaporation takes place predominantly from states of relatively high spin, but yet considerably below the value $l_{max} = 190\ \hbar$ in the entrance channel.

This discussion is all based on the assumption of ^{4}He emission early in the deexcitation cascade. Our evidence is clear that most observed ^{4}He emission does precede full fragment acceleration, and even scission itself. In addition, the total multiplicity of ^{4}He emission is less than unity. Thus one would expect that each deexcitation chain would usually give zero or one ^{4}He particle. An extension of this reasoning to include pre-scission neutron and H emission (next paragraphs) would indicate pre-scission cascades of one to five particles. For average initial spins of ≤ 100 for the ^{237}Bk, such cascades would not be expected to bring the system very near to the Yrast line. Thus we do not expect H/He emission from near-Yrast states to greatly alter the above analysis.

If we grant that the energy and angular distributions for H/He emission (at back angles) imply emission from an essentially equilibrated system, then it is natural to ask if an equilibrium model can account for the ratio of particle emission to fission ($\Gamma_f : \Gamma_\alpha : \Gamma_p \approx 3:1:1$). Quite simply the answer is negative. The calculated fission barrier for ^{237}Bk is ≈2 MeV for $I = 0$ and is reduced to near zero for spins of several tens.[35] The sum of proton or alpha binding energy plus Coulomb barrier is ≈14 MeV (see Table VIII). Thus for $T \approx 2.5$ MeV we can expect Γ_α/Γ_f or $\Gamma_p/\Gamma_f \approx \exp(-14/2.5) \cong 0.004$. Clearly the composite nucleus is not choosing its decay probabilities by counting open channels as in the Boltzmann equation. We infer that the energy sharing among particles must be very fast and even after this extensive mixing the intrinsic particle decay rates must be fast enough for significant particle evaporation to occur prior to scission (about one proton and α per 3 fissions).[43,44] This effect may simply reflect non-participation of the fission channels in the equilibrium model rather than its complete demise.[12,44-46] The dynamic trajectory calculations of Nörenberg and Riedel[37] provide a possible way to account for our observations above. They point out that a dinuclear complex, such as ^{40}Ar + ^{197}Au, could be trapped in a potential well for $l \cong 100$ and this complex could survive for more than one rotation period while mass diffusion moves the complex closer towards mass symmetry. During the time of extensive mass diffusion, the possibility exists for evaporative emission prior to the scission of the ultimately unstable complex.

It is interesting to digress briefly from our major track to explore more fully the implications of the Boltzmann equation for emission of neutrons, protons, and alphas. In Table VIII we list the particle separation energies[47] and emission Coulomb barriers for the nucleus ^{237}Bk and for some typical fission products. If we assume that the most probable charge to mass ratio of the primary fragments is 97/237 then ^{86}Br, ^{118}Cd, and

TABLE VIII. Separation energies[a] S_x and Coulomb barriers[b] B_x (all energies in MeV).

	$^{237}_{97}$Bk	$^{86}_{35}$Br	$^{78}_{35}$Br	$^{118}_{48}$Cd	$^{110}_{48}$Cd	$^{151}_{62}$Sm	$^{141}_{62}$Sm
E^*	160	73	5	110	20	127	25
S_n	8	5.4	8.3	8.4	9.9	5.6	8.5
S_p	2	9.6	6.7	11.1	8.9	8.3	5.0
B_p	11	4.7	4.7	6.0	6.0	7.3	7.3
S_p+B_p	13	14.3	11.4	17.1	14.9	15.6	12.3
S_α	−8	8.4	5.0	4.9	2.8	1.2	−0.8
B_α	23	9.0	9.0	12.0	12.0	13.5	13.5
$S_\alpha+B_\alpha$	15	17.4	14.0	16.9	14.8	14.7	12.7

[a] The subscripts "x" are n for neutron, p for ^{1}H, and α for ^{4}He. Separation energies were computed from Ref. 47.

[b] Coulomb barriers were estimated from Ref. 19.

^{151}Sm would be typical primary fragments ($T \approx 2.5$ MeV). ^{78}Br, ^{110}Cd, and ^{141}Sm would then correspond to products near the end of the neutron evaporation cascade ($T \approx 1$ MeV). For ^{237}Bk one would estimate $\Gamma_n : \Gamma_p : \Gamma_\alpha \approx 1 : \exp[-(S_p + B_p - S_n)/T] : \exp[-(S_\alpha + B_\alpha - S_n)/T] = 1 : e^{-2} : e^{-3}$ or ≈5 neutrons per (H + He). This estimate is not expected to be very precise but it does suggest significant emission of pre-scission neutrons in addition to pre-scission H/He.[45,46] For the primary fragments ^{86}Br, ^{118}Cd, and ^{151}Sm one might estimate Γ_{H+He}/Γ_n to be, respectively, 0.036, 0.064, and 0.044. For the cooler fragments ^{78}Br, ^{110}Cd, and ^{141}Sm these ratios may be, respectively, 0.048, 0.014, and 0.037. Thus for a postfission evaporation cascade of 8–10 emission steps, a significant amount of H/He emission should occur. We infer that these processes are masked by the apparently more abundant pre-scission emissions.

Let us turn now to the forward-peaked or direct component of the particle emission. For the system ^{40}Ar + ^{77}Se → ^{117}Te, Galin *et al.* observed no direct components for H or He.[9] This suggests that either the direct component for ^{117}Te was masked by the evaporation (and escaped detection) or that for our ^{237}Bk system the high charge, excitation, and/or spin gives rise to more prominent direct emission. Further, for ^{237}Bk the Z distribution of the heavy products in coincidence with these direct emissions is indistinguishable from that for the evaporation component (90% of emissions have $27 < Z < 70$ and the values of $\langle Z \rangle$ are equivalent). Thus it appears that many of these direct reactions are accompanied by fusion of the projectile residue with the target and a subsequent fission-like breakup.[48] Such a process is very similar to that reported in Refs. 10, 11, 13, 14, and 49 and termed massive transfer or *transfert très inelastique*.

The out-of-plane correlation for the forward-peaked ^{4}He ejections is even stronger than for the evaporation-like component (Fig. 6 and Table V). In Tables V and VI we give a summary of the out-of-plane data, grouped in such a way as to separate forward and backward emissions and to show the statistical significance. The coincidence cross sections for ^{4}He decrease strongly as one moves away from the reaction plane which would seem to reflect very large entrance-channel spins. Surprisingly the coincidence cross sections for ^{1}H seem to increase as one moves out of the reaction plane. This increase is only about two standard deviations and could, of course, be only an illusion of the counting statistics. However, the first and second moments of the observed energies ($\langle \epsilon \rangle$ and σ_ϵ) also indicate a trend reversal between ^{1}H and ^{4}He. In Table VI one can see that the values of $\langle \epsilon \rangle$ and σ_ϵ ($\theta_{c.m.} < 60°$) are greater for ^{4}He in the reaction plane and for ^{1}H out of the plane. This is consistent with a larger presence of direct emission in the plane for ^{4}He and out of the plane for ^{1}H (see Fig. 6 as well). This pattern seems to us to be very interesting and surprising and should be investigated further with much better statistics.

In the Appendix we describe one possible mechanism for the strange behavior of the ^{1}H emissions. As the ^{4}He direct emission decreases with increasing φ, we suspect that its major driving force is a large spin of the composite system perpendicular to the reaction plane. Equations (2) or (11) based on equilibrium considerations must fail in detail for the out-of-plane correlation. Nevertheless, one might consider this suggestive that the direct emissions arise from larger partial waves. If the projectile-like fragments are formed for $140 < l < 190$, then possibly the forward-peaked ^{4}He is formed for l waves approaching 140. Centrifugal effects could enhance their out-of-plane correlation and their average energies.

The energy spectra of the forward-peaked component for ^{4}He can be examined in more detail by subtraction of an assumed symmetric component. Such a subtraction reveals two distinct aspects of these forward-peaked emissions (Fig. 3): First the high-temperature component (H) with $T \approx 3$–7 MeV is obvious (Figs. 1, 2, and 7 and Tables I and VI), but also there is significant forward peaking in the near-barrier part of the spectrum (L) with most probable $\epsilon_\alpha \approx 23$ MeV and $\epsilon_H \approx 12$ MeV. The high-energy component may well reflect memory of the projectile velocity as in Refs. 10, 11, 13, and 14. The low-energy component would seem to reflect considerable energy sharing among particles even for these forward-peaked emissions.

As shown by the separation and Coulomb ener-

gies in Table VIII, any phase space calculation would be expected to favor fission over H/He emission by much more than the observed ratios. We have been driven to the conclusion that the intrinsic rate of H/He emission is faster than the time of several nanopicoseconds required to arrive at the scission point.[43] This is not surprising for the very high speed forward-peaked emission of clearly preequilibrium character.[44] It *is* surprising for the backward emission that shows temperatures and angular distributions consistent with evaporation, and these observations may be evidence in support of the mechanistic predictions of Nörenberg and Riedel.[37] If both direct and evaporative H/He emission are bleeding away spin, charge, and energy from the higher spin composite nuclei, this could strongly influence the fission probability for lower Z systems.[12] For a high Z system, such as ^{237}Bk, fission would be expected to occur even after He emission. For ^{194}Hg and lighter systems studied earlier, the fission process might be aborted by this phenomenon,[29] and phase space interpretations may be led astray.[50,51]

The implications of this study are quite important for reaction phenomena between complex nuclei. Even prior to the very rapid fission and quasifission processes,[52] "quasifusion" and "quasievaporation" must be taking place. These processes as well as their forward-peaked preequilibrium cousins[53] provide a means of studying the reaction process on a time scale comparable to that for energy damping in the entrance channel.

V. SUMMARY AND CONCLUSIONS

We now attempt to collect the various mechanistic suggestions that emerge from the literature and from this work. Of the ≈2500 mb reaction cross section for 340-MeV ^{40}Ar + Au, ≈1400 mb goes to totally relaxed fission-like products of $27 < Z < 70$. The remaining ≈1100 mb is presumed to lead to projectile-target-like breakups via quasielastic and very inelastic reactions. Of the ≈190 reactive partial waves in the entrance channel, the latter reactions are expected to dominate the highest ≈50 partial waves and the former probably dominate from $0 < l <$ ~140. The total cross section for H + He is ≈1500 mb with emission predominantly preceding scission into fission-like fragments of $27 < Z < 70$. Most of this H/He emission exhibits low temperatures (≈2.5 MeV) and seems to derive from an energy equilibrated system. However, significant forward peaking is observed for both a high-temperature component ($T \approx 3$–7 MeV) and for ^{1}H/He with near-barrier energies. A strict statistical equilibrium model could not account for such high cross sections for evaporated H/He in comparison to fission from ^{237}Bk of relatively high spin and low fission barrier. It would appear that energy mixing among the particles and even quasievaporation must occur in times comparable to that for the scission time of several 10^{-21} seconds. If the Boltzmann equation is applicable for the ratio of neutron to alpha quasievaporation, one would infer that several neutrons would usually be emitted prior to scission. From the analysis of the angular distributions, it appears that low-temperature ^{4}He emission occurs from composite nuclei of $\langle (I + \frac{1}{2})^2 \rangle^{1/2} \approx 70\hbar$ and higher-temperature emission may come from even higher spin states. The backward ^{1}H emission seems to be nearly isotropic and, as the expected exit-channel l values are small, no definite information on spins can be obtained from that source. The very fast H/He emissions seem to provide an interesting tool for investigating the energy mixing in reactions between complex nuclei and thus the very early history of the composite system.

ACKNOWLEDGMENTS

The staff of the SuperHILAC accelerator at the Lawrence Berkeley Laboratory has been very cooperative. Special thanks are due to H. Delagrange, E. Duek, H. Grunder, C. Maples, and M. F. Rivet for helpful discussions and continued interest in our work. This project was supported by the Division of Nuclear Physics of the U. S. Department of Energy.

APPENDIX

As mentioned above, the anisotropy for H emission (singles mode, $\theta_{c.m.} > 100°$) is not visible in Fig. 4; presumably it is small although it could have been masked by a gradual intrusion of forward-peaked direct processes. The out-of-plane correlation for ^{1}H seems to suggest a preference for out-of-plane emission (see Fig. 6 and Table V). However, this suggestion is based on about two standard deviations from isotropy and should not be taken as a definitive observation without further study.

These observations, tentative as they are, stimulate us to search for a possible cause. Imagine that the H emission takes place on a time scale slow enough for extensive energy sharing but considerably faster than that for the collective motions leading to scission and complete fragment acceleration. In addition, imagine that most H emission takes place from a neck region between the fragments, and their Coulomb fields focus the H into a plane perpendicular to the line between the fragment

centers. Substantial rotation of this line of centers, prior to full acceleration of the fragments, would give a set of planes that share a common emission direction perpendicular to the reaction plane. In the limit of long rotation times, emission probability would follow $1/\sin(90^\circ - \varphi)$ just analogous to the very familiar $1/\sin\theta$ limit for fission.

Note that for ^{4}He emission the expected out-of-plane correlation was observed; this calls for composite-nucleus spin as a correlating force. For ^{40}Ar + Au there is apparently no preferential emission of He perpendicular to the final axis of fragment separation (see Fig. 6 and Table VII). Therefore, if the emission is from the neck, it must occur over the time period required to rotate $\approx 180^\circ$ or without much focusing by the nascent fragments. This could imply that H and He may be emitted at different ages of the evolving system.

[1]W. J. Knox, A. R. Quinton, and C. E. Anderson, Phys. Rev. 120, 2120 (1960).
[2]C. E. Hunting, Phys. Rev. 123, 606 (1961).
[3]H. C. Britt and A. R. Quinton, Phys. Rev. 124, 877 (1961).
[4]D. V. Reames, Phys. Rev. 137, B332 (1965).
[5]F. E. Durham and M. L. Halbert, Phys. Rev. 137, B850 (1965).
[6]A. Kapuszik, V. P. Perelygin, S. P. Tret'yakova, and L. V. Ukraintseva, Yad. Fiz. 6, 1142 (1967) [Sov. J. Nucl. Phys. 6, 829 (1968)].
[7]C. Brun, B. Gatty, M. Lefort, and X. Tarrago, Nucl. Phys. A116, 177 (1968).
[8]R. C. Reedy, M. J. Fluss, G. F. Herzog, L. Kowalski, and J. M. Miller, Phys. Rev. 188, 1771 (1969); J. M. D'Auria, M. J. Fluss, G. Herzog, L. Kowalski, J. M. Miller, and R. C. Reedy, *ibid.* 174, 1409 (1968).
[9]J. Galin, B. Gatty, D. Guerreau, C. Rousset, U. C. Schlotthauer-Voos, and X. Tarrago, Phys. Rev. C 9, 1113 (1974); 9, 1126 (1974); 10, 638 (1974).
[10]T. Inamura, M. Ishihara, T. Fukuda, and T. Shimoda, Phys. Lett. 68B, 51 (1977).
[11]T. Nomura, H. Utsunomiya, T. Motobayashi, T. Inamura, and M. Yanokura, Phys. Rev. Lett. 40, 694 (1978).
[12]J. M. Miller, D. Logan, G. L. Catchen, M. Rajagopalan, J. M. Alexander, M. Kaplan, J. W. Ball, M. S. Zisman, and L. Kowalski, Phys. Rev. Lett. 40, 1074 (1978), and unpublished data from the same group.
[13]D. R. Zolnowski, H. Yamada, S. E. Cala, A. C. Kahler, and T. T. Sugihara, Phys. Rev. Lett. 41, 92 (1978); H. Yamada, D. R. Zolnowski, S. E. Cala, A. C. Kahler, J. Pierce, and T. T. Sugihara, *ibid.* 43, 605 (1979).
[14]D. G. Sarantites, L. Westerberg, M. L. Halbert, R. A. Dayras, D. C. Hensley, and J. H. Barker, Phys. Rev. C 18, 774 (1978); K. A. Geoffroy, D. G. Sarantites, M. L. Halbert, D. C. Hensley, R. A. Dayras, and J. H. Barker, Phys. Rev. Lett. 43, 1303 (1979).
[15]A. Gamp, J. C. Jacmart, N. Poffé, H. Doubre, J. C. Roynette, and J. Wilczynski, Phys. Lett. 74B, 215 (1978); A. Gamp, H. L. Harney, J. C. Roynette, E. Plagnol, H. Fuchs, H. Doubre, J. C. Jacmart, and N. Poffé, Z. Phys. A291, 347 (1979).
[16]J. M. Blatt and V. F. Weisskopf, *Theoretical Nuclear Physics* (Wiley, New York, 1952).
[17]H. A. Bethe, Rev. Mod. Phys. 9, 71 (1937).
[18]T. Ericson, Adv. Phys. 9, 423 (1960).
[19]M. A. McMahan and J. M. Alexander, Phys. Rev. C 21, 1261 (1980).
[20]T. Ericson and V. Strutinski, Nucl. Phys. 8, 284 (1958); 9, 689 (1959).
[21]T. Døssing (unpublished).
[22]G. L. Catchen, M. Kaplan, J. M. Alexander, and M. F. Rivet, Phys. Rev. C 21, 940 (1980).
[23]J. M. Miller, G. L. Catchen, D. Logan, M. Rajagopalan, J. M. Alexander, M. Kaplan, and M. S. Zisman, Phys. Rev. Lett. 40, 100 (1978).
[24]G. L. Catchen, D. Logan, J. M. Miller, D. Benson, N. H. Lu, T. W. Debiak, M. Rajagopalan, J. M. Alexander, M. Kaplan, and M. S. Zisman (unpublished).
[25]J. W. Harris, T. M. Cormier, D. F. Geesaman, L. L. Lee, Jr., R. L. McGrath, and J. P. Wurm, Phys. Rev. Lett. 38, 1460 (1977).
[26]R. Albrecht, W. Dünnweber, G. Graw, H. Ho, S. G. Steadman, and J. P. Wurm, Phys. Rev. Lett. 34, 1400 (1975); H. Ho, R. Albrecht, W. Dünnweber, G. Graw, S. G. Steadman, J. P. Wurm, D. Disdier, V. Rauch, and F. Scheibling, Z. Phys. A283, 235 (1977).
[27]C. K. Gelbke, M. Bini, C. Olmer, D. L. Hendrie, J. L. Laville, J. Mahoney, M. K. Mermaz, D. K. Scott, and H. H. Weiman, Phys. Lett. 71B, 83 (1977); P. Dyer, T. C. Awes, C. K. Gelbke, B. B. Back, A. Mignerey, K. L. Wolf, H. Breuer, V. E. Viola, Jr., and W. G. Meyer, Phys. Rev. Lett. 42, 560 (1979).
[28]I. Halpern, Annu. Rev. Nucl. Sci. 21, 245 (1971).
[29]N. Carjan, A. Sundulescu, and V. V. Pashkevich, Phys. Rev. C 11, 782 (1975); N. Carjan, J. Phys. (Paris) 37, 1279 (1976); N. Carjan, dissertation, Technischen Hochschule Darmstadt, 1977 (unpublished).
[30]M. Rajagopalan and T. D. Thomas, Phys. Rev. C 5, 1402 (1972); 5, 2064 (1972) and references therein.
[31]L. G. Moretto, J. Galin, R. Babinet, Z. Fraenkel, R. Schmitt, R. Jared, and S. G. Thompson, Nucl. Phys. A259, 173 (1976).
[32]C. Ngô, J. Peter, B. Tamain, M. Berlanger, and F. Hanappe, Z. Phys. A283, 161 (1977).
[33]J. Galin, B. Gatty, D. Guerreau, M. Lefort, X. Tarrago, S. Agarwal, R. Babinet, B. Cauvin, J. Girard, and H. Nifenecker, Z. Phys. A283, 173 (1977).
[34]R. Lucas, J. Poitou, H. Nifenecker, J. Peter, and B. Tamain, Z. Phys. A283, 257 (1977).
[35]S. Cohen, F. Plasil, and W. J. Swiatecki, Ann. Phys. (N.Y.) 82, 557 (1974).
[36]B. Tamain, C. Ngô, J. Peter, and F. Hanappe, Nucl. Phys. A252, 187 (1975), and references therein.
[37]W. Nörenberg and C. Riedel, Z. Phys. A290, 335

(1979).
[38]M. M. Fowler and R. C. Jared, Nucl. Instrum. Methods 124, 341 (1975).
[39]S. B. Kaufman, E. P. Steinberg, B. D. Wilkins, J. Unik, A. J. Gorski, and M. J. Fluss, Nucl. Instrum. Methods 115, 47 (1974).
[40]L. C. Northcliffe and R. G. Schilling, Nucl. Data Tables A7, 223 (1970).
[41]J. R. Birkelund, J. R. Huizenga, H. Freiesleben, K. L. Wolf, J. P. Unik, and V. E. Viola, Jr., Phys. Rev. C 13, 133 (1976).
[42]Kinematic calculations carried out by T. W. Debiak, A. Fleury, and M. F. Rivet using a Monte Carlo method show that isotropic evaporation from fission fragments [$W(\theta) \propto (1/\sin\theta)$] leads to a broad, relatively flat energy distribution of width $\approx$32 MeV for ^{4}He. The results of these calculations at several laboratory angles for ^{4}He and ^{1}H emission are shown in Fig. 9.
[43]J. R. Nix, Argonne National Laboratory Report No. ANL/PHY/76-2, Vol. I (1976).
[44]M. Blann, Nucl. Phys. A235, 211 (1974).
[45]E. Cheifetz, Z. Fraenkel, J. Galin, M. Lefort, J. Peter, and X. Tarrago, Phys. Rev. C 2, 256 (1970).
[46]G. N. Harding and F. J. M. Farley, Proc. R. Phys. Soc. London A69, 853 (1956).
[47]A. H. Wapstra and N. B. Gove, Nucl. Data A9, 265 (1971).
[48]L. Kowalski, J. M. Alexander, D. Logan, M. Rajagopalan, M. Kaplan, M. S. Zisman, and T. W. Debiak, unpublished data on linear momentum transfer in this system.
[49]M. F. Rivet, These d'Etat, Orsay, 1977 (unpublished).
[50]M. Beckerman and M. Blann, Phys. Rev. Lett. 38, 272 (1977); Phys. Lett. 68B, 31 (1977).
[51]H. Delagrange, A. Fleury, and J. M. Alexander, Phys. Rev. C 16, 706 (1977).
[52]U. Schröder and J. R. Huizenga, Annu. Rev. Nucl. Sci. 27, 465 (1977).
[53]J. P. Bondorf, J. N. De, A. O. T. Karvinen, G. Fai, and B. Jakobsson, Phys. Lett. 84B, 162 (1979).